Constrained Design of Potentiometric RFID Sensors Based on Auto-Tuning ICs

F. Nanni and G. Marrocco, *Senior Member, IEEE*

***Abstract*— Auto-Tuning Integrated Circuits (ICs), interconnected with Radiofrequency Identification (RFID) antennas in the UHF band, can provide digital information about the changes in the local boundary conditions in the proximity of the device. This feature, in conjunction with a varactor diode, can be used to create a general purpose framework for the controlled wireless sensing of chemical agents. The varactor works as a transducer converting the potentiometric output of a chemical sensor into a capacitance change, which in turn is detected by the IC. A constrained optimization method is here introduced to maximize the sensitivity of the above transduction mechanism by deriving closed-form expressions that relate the digital output of the IC to the chemical variation. In this way, said variation will be optimally mapped within the retuning dynamic range of the IC. The method is demonstrated with reference to a pH sensor and is capable of providing a sensitivity of 30 units per unitary pH variation with stable communication performance. Moreover, the application to an on-body plaster-like antenna, namely when there are not fully controllable boundary conditions, demonstrated that the sensing performance is practically unaffected by the placement region over the human body as well as by the inter-user variability.**

***Index Terms*— RFID, Auto-Tuning antennas, constrained design, chemical potentiometric sensing, pH.**

I. Introduction

WEARABLE and Epidermal sensors have attracted considerable interest in recent years since they allow noninvasive real-time monitoring of electrolytes and metabolites contained in biological fluids such as sweat, tears, or saliva as indicators of the wearer's health status. In particular, parameters such as pH, glucose, lactate, cholesterol, potassium, calcium, and metal ions, combined with physical data such as activity, body temperature, and heart rate can greatly improve the chances of detecting adverse health conditions, like infections of implanted devices [1], [2] or superficial chronic wounds [3], [4], [5], [6].

For maximum flexibility, data collection is nowadays expected to be wireless and hopefully batteryless. For this purpose, a transceiver antenna, an energy harvesting circuit, and a low-power digital modulation circuit were used in [7] to create a passive pH sensor, which converts the analog voltage into an 8-bit word. The work in [8] describes a stretchable wireless device comprising a potentiometric pH sensor made by a graphite-polyurethane composite and an Ag/AgCl reference electrode. pH data is continuously transmitted to a smartphone through a short-range Radio Frequency Identification (RFID) link in the HF band. A medium-range wireless interrogation was instead achieved in [9] through RFID in the UHF band (860-960 MHz), using a small wireless flexible pH sensor for integration with an epidermal antenna and a now-discontinued sensor-oriented RFID Integrated Circuit (IC). In the above papers, the ICs are almost always equipped with an inbuilt Analog to Digital Converter (ADC).

Francesca Nanni and Gaetano Marrocco are both with the Pervasive Electromagnetics Lab, University of Rome Tor Vergata, Italy (email: frmach97@gmail.com, gaetano.marrocco@uniroma2.it).

A different sensing method relies on a new family of auto-tuning microchips that can autonomously adjust their internal RF admittance to make IC-antenna matching rather insensitive to changes in the local boundary conditions [10].

The potentialities of auto-tuning ICs have been recently investigated to convert the variation of some physical parameter nearby the antenna, for instance to estimate the temperature variation as in [11], by inducing a mismatch of the antenna through the changing of the substrate and metallic parts. In [12] the auto-tuning architecture was exploited to derive fingertip-worn epidermal sensors, in the framework of the emerging Tactile Internet, to detect the content of bottles by optimizing the antenna behavior on variable dielectrics. Similarly, the application to the estimation of the moisture content into a face-mask [13] leverages the local increase in the mask permittivity during prolonged breathing. Finally, the auto-tuning IC has been also proposed for the potentiometric sensing itself by exploiting a varactor diode as a conditioning circuit that, in reaction to external stimuli, can change the IC-antenna matching, thus activating the auto-tuning process that returns a code proportional to the retuning effort. The idea was applied to the wireless monitoring of AC currents [14] where the detected reactance value is transmitted as a 5-bit code that is directly related to the AC current drawn by an electrical load. Finally, by exploiting the above features, chemical-interacting materials (PDMS) were used in [15] and [16] to convert the value of pH and other electrolytes into a variation of electric permittivity of such material and, in turn, of the capacitance of an electrode.

The main limitation of the above works, concerning the use of auto-tuning ICs with potentiometric quantities, is the lack of control over performance parameters, namely, the device performances are taken as they are, without any possibility to

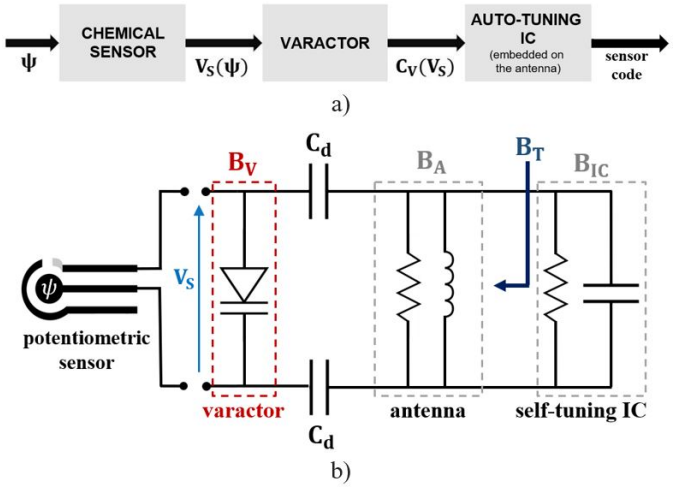

Fig. 1. a) Block Diagram of the RFID-based potentiometric sensor; b) equivalent circuit.

shape the dynamic range and resolution of the output data.

By extending the preliminary ideas in [17], this paper proposes a design methodology that is instead suitable to gain full control of the mapping of the potentiometric output of a chemical sensor onto the available range of the auto-tuning RFID IC. In particular, we are interested in maximizing the sensitivity to chemical parameters and in enabling the reconfigurability of the device's response by minimal changes of few conditioning lumped elements. For this purpose, we have discovered that the antenna of the device is the key point in the mapping since, by a proper design, it can be involved in the physical-to-digital conversion. In other words, the requirements on the sensing process are partly converted in antenna design constraints.

Accordingly, a rigorous closed-form model of the whole sensing chain, accounting for the sensor, the varactor diode working as a transducer, and the auto-tuning IC is derived, and a constrained optimization problem for the antenna shape, communication, and sensing requirements is formulated. The purpose is to drive the optimal design of said antenna so that the whole range of the chemical agent is captured as needed, while preserving the communication performance.

This paper is organized as follows: Section II introduces the physical rationale of the method while the constraints on the antenna design are given in Section III, together with the mapping conditions for the specific design. Section IV describes the degrees of freedom that dominate the system's sensitivity and the whole method is applied to a reference device in Section V with the help of numerical simulations and measurements on prototypes. Finally, an application example is given in Section VI concerning a flexible and soft epidermal electronic plaster for skin monitoring, with the purpose to quantify the robustness of the method versus variable placement conditions.

II. Rationale of Auto-Tuning IC as Potentiometric Sensor

The functional modules of the considered sensing architecture, and the corresponding interactions, are sketched in Fig.1 a). The voltage generated by the potentiometric chemical sensor causes a change in the diode's internal junction capacitance, which will induce a mismatch with the microchip's admittance. In turn, the microchip will self-adapt, and in doing this, it generates a digital information related to the input chemical quantity. The models of the relevant modules are reported next.

A. Self-tuning RFID ICs

A model of auto-tuning RFID ICs [10] assumes an adaptive internal capacitor, with overall capacitance:

$$C_{IC}(s) = C_{min} + sC_0 \tag{1}$$

with C_{min} and C_0 being specific parameters of the IC.

The integer number "s", hereafter referred to as sensor code, is generated by the IC (Fig.1 b)) and transmitted to the reader by the antenna, following the usual backscattering modulation. In particular, by collecting the impinging electromagnetic field coming from the reader, the IC activates, evaluates the sensor code and stores it in a proper memory bank, that is then read by the reader following a further specific query.

Auto-tuning activates so that the sum of the susceptances of the IC ($B_{IC}(s) = \omega C_{IC}(s)$) and that of the connected antenna (B_A) is forced to be zero, namely:

$$B_{IC}(s) + B_A = 0. \tag{2}$$

The auto-tuning effort of the IC is generally limited so that the sensor code is constrained within a finite set. It is encoded with N bits so that it will formally span between $s = 0$ and $s = 2^N - 1$. In case of more severe mismatch, the sensor code saturates to the boundaries above [12]. However, to make the IC operate in linear mode, the meaningful range of the sensor code is smaller. For the sake of generality, we will hereafter consider the subset $S_{min} < s < S_{max}$, being $S_{min} \geq 0$ and $S_{max} \leq 2^N - 1$, whose values are dependent on the specific IC implementation.

B. The varactor diode as transducer

Let's now consider the network in Fig.1 b) wherein a varactor diode is interconnected in parallel with the antenna, the IC, and the potentiometric sensor. Denoting with ψ the chemical agent to be observed, the sensor generates a voltage in response to a given value of ψ, namely $V_S(\psi)$. Moreover, two identical capacitances C_d are introduced between the varactor and the remaining part of the circuit, aiming at decoupling the IC and the diode since they operate at different frequencies (the sensor feeds the diode in DC while the antenna operates in RF). As shown later on, this parameter will provide additional degrees of freedom in the sensor design.

The total susceptance B_T seen by the IC toward the remaining part of the network is:

$$B_T(\psi) = B_A + \frac{B_V(\psi) \cdot \omega C_d}{2B_V(\psi) + \omega C_d}. \tag{3}$$

B_V is the susceptance of the varactor diode which is controlled by the sensor as:

$$B_V[V_S(\psi)] = B_V(\psi) = \omega C_J(\psi) = \frac{\omega C_{j0}}{(1 + \frac{V(\psi)}{V_J})^M} \tag{4}$$

where C_J is the junction capacitance and $\{C_{j0}$, M, $V_J\}$ are the capacitance of the un-polarized diode, a constant dependent on the material, and the barrier potential [18], respectively.

The auto-tuning condition (2) will still hold by replacing B_A with B_T. Accordingly, by combining (1) with (2) the sensor code returned by the IC is:

$$s(\psi) = nint[-\frac{1}{C_0}(C_{IC,min} + \frac{B_A}{\omega} + \frac{B_V(\psi)\cdot C_d}{2B_V(\psi)+\omega C_d})] \quad (5)$$

where the operator "*nint*" is a quantization operator that approximates its argument to the nearest integer number. Overall the following mapping is established:

$$\psi \rightarrow V \rightarrow s. \quad (6)$$

The overall performance of the sensing chain, namely the measurement range and its resolution, depend on the selection of both the specific chemical sensor and the diode:

1) The choice of the chemical sensor is driven by the pH range of interest. The output voltage range is accordingly determined;
2) The diode must have a voltage interface that is compatible with the sensor output and possibly the highest slope of the characteristic curve ($V - C_J$) to maximize the measurement resolution.

Finally, the selection of the substrate is dependent on the target object, namely a flexible and hopefully elastic membrane for application onto the human skin, while more rigid substrates can be used in case of hard and flat targets.

C. Quantization error

The analog-to-digital (ADC) conversion occurs at the varactor-IC interface and induces a quantization error. Practically, the IC digitalizes the capacitance of the varactor and the quantization error propagates to the input of the varactor, namely the voltage produced by the sensor. By considering a linearization of (5) (just before the "nint" operation) around the condition of the unloaded sensor ($V_S = 0$, so that, from (4) $B_V(0) = \omega C_{j0}$), the resolution in the measurement of the B_V is given by $\delta B_V = \frac{\delta s}{|m|}$, where $\delta s = 1$ is the resolution of the sensor code, and m is the slope of the linearized curve, namely:

$$m = \frac{ds}{dB_V} = -k\frac{C_d^2}{aC_d^2 + bC_d + c} \quad (7)$$

where $k = \frac{\omega}{C_0}$, $a = \omega^2$, $b = 4\omega^2 C_{j0}$, $c = 4\ \omega^2 C_j^2$.
The quantization error is, hence, $e_{B_V} = \frac{q}{2} = \frac{1}{2|m|}$ and depends on the decoupling capacitance C_d. Furthermore, once fixed the frequency and the diode model, e_{B_V} will approach the limit $e_{B_V} \rightarrow \frac{a}{2k}$ for $C_d \rightarrow \infty$ that is hence the lower-bound of the quantization error. Overall, the capacitor C_d permits to tune the quantization of the potentiometric sensor so that a lower error can be achieved by means of higher values of the decoupling capacitance. Moreover, the increases of C_d (rise of the slope m) is also beneficial for the widening of the dynamic range of the sensing parameter that can be mapped onto the available set of sensor codes, as will be shown in the next Section.

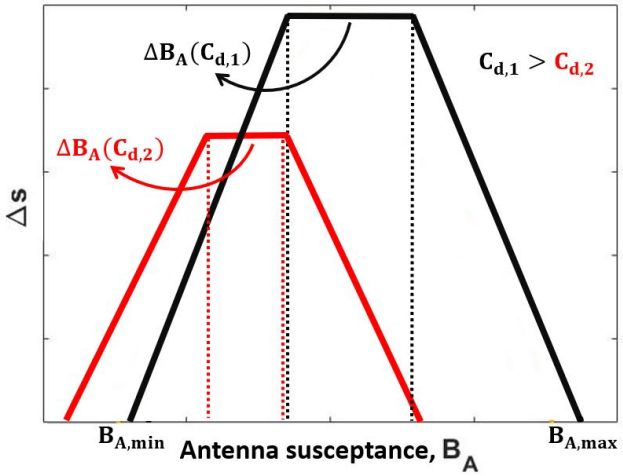

Fig. 2. Qualitative representation of the achievable sensor code contrast $\triangle s = s(V_{S,max}) - s(V_{S,min})$ as a function of the antenna susceptance for two values of C_d ($C_{d,1} > C_{d,2}$).

III. Voltage Mapping on the Sensor Code

A. Problem formulation

Equation (6) establishes a link between the chemical agent to be monitored and the RFID IC output. The key idea is to map the entire expected variation of the parameter to measure (the voltage produced by the specific sensor polarizing the varactor) just inside the useable range of the sensor code, thus exploiting the maximum transduction sensitivity and avoiding saturation.

For this purpose, let's fix the varactor model, the IC, and the range $\psi_{min} \leq \psi \leq \psi_{max}$ of the chemical agent. The $\psi - s$ mapping can be controlled from (5) by acting on the design of the antenna, namely by enforcing the proper susceptance B_A. In the specific, by assuming without loss of generality that the characteristic curve $\psi - V_S$ has a negative slope (namely the increase of the chemical agent produces a reduction of the voltage), the range of existence $[V_{S,min}, V_{S,max}]$ of V_S is:

$$V_{S,min} = V_S(\psi_{max}), \qquad V_{S,max} = V_S(\psi_{min}) \quad (8)$$

and similarly for $B_{V,min}$ and $B_{V,max}$.

It is easily shown that the antenna admittance must be constrained within $B_{A,min} \leq B_A \leq B_{A,max}$, where:

$$\begin{cases} B_{A,min} = -B_{IC}(S_{max}) - \frac{B_{V,max}\cdot\omega C_d}{2B_{V,max}+\omega C_d} \\ B_{A,max} = -B_{IC}(S_{min}) - \frac{B_{V,min}\cdot\omega C_d}{2B_{V,min}+\omega C_d}. \end{cases} \quad (9)$$

Let's now introduce the sensor code contrast $\triangle s = s_{max} - s_{min}$, namely the overall achieved variation of the sensor code corresponding to the range of ψ of interest. Fig.2 shows a qualitative representation of the mapping as the antenna susceptance increases within the above-mentioned range for two values of the decoupling capacitance ($C_{d,1} > C_{d,2}$). The sensor code contrast $\triangle s$ linearly widens along with the value of B_A until a maximum value, $\triangle s_{max}$, is reached so that an optimal sub-range of B_A is identified. The peak value for $\triangle s$ increases with the capacitance C_d, and there is a widening of the corresponding interval of the useful antenna susceptance. The device sensitivity can be defined as $S(\psi) = \frac{\triangle s}{\psi_{max} - \psi_{min}}$.

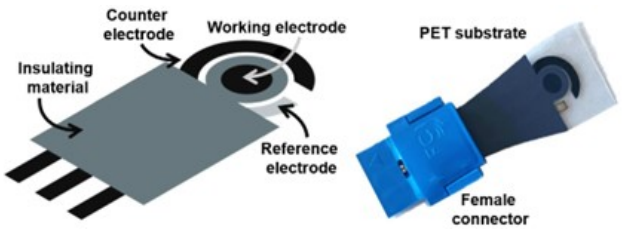

Fig. 3. a) Schematic and b) real picture of the pH sensor. The bulky connector (blue) is used to quickly plug and remove it from the device.

B. Penalty Function

Let's denote with $\underline{\alpha} = \{\alpha_1, .., \alpha_M\}$ some geometrical parameters of the antenna determinating its shape, or electrical parameters related to eventual lumped electrical devices (such as inductors or capacitors) to provide additional freedom of the antenna.

The range mapping, also accounting for the maximization of the realized gain for communication purposes, can be cast as the minimization of the following penalty function:

$$U[\underline{\alpha}] = \sum_{i=1}^{3} w_i u_i[\underline{\alpha}] \tag{10}$$

where:

$$u_1 = \begin{cases} \left|1 - \frac{|B_A(\psi_{max})[\underline{\alpha}]|}{\omega C_{IC}(S_{min})}\right| \\ if\ C_{IC}(S_{min}) \leq -\frac{B_A(\psi_{max})}{\omega} \leq C_{IC}(S_{max}) \\ 1\ otherwise \end{cases} \tag{11}$$

$$u_2 = \begin{cases} \left|1 - \frac{|B_A(\psi_{min})[\underline{\alpha}]|}{\omega C_{IC}(S_{max})}\right| \\ if\ C_{IC}(S_{min}) \leq -\frac{B_A(\psi_{min})}{\omega} \leq C_{IC}(S_{max}) \\ 1\ otherwise \end{cases} \tag{12}$$

$$u_3 = \frac{G_0}{\widetilde{G}}. \tag{13}$$

The first two sub-penalties u_1 and u_2 enforce the mapping of the device susceptance inside the useful auto-tuning range. The sub-penalty u_3 maximizes the realized gain $\widetilde{G} = G\tau$ in linear scale of the antenna (being τ the power transfer coefficient between the antenna and the IC) and G_0 a normalization parameter so that $0 \leq u_3 \leq 1$. The weights w_i are such that $\sum_j w_j = 1$ [12].

The penalty function U_i is evaluated for a choice of the weights such to balance both the sensing mapping ($w_1 = w_2 = 1/4$) and the communication performance ($w_3 = 1/2$). The reference gain was set to 1/10. The antenna gain and admittance are computed numerically.

It is worth expecting that the constrained optimization will probably lead to a partial use of the useful range of the sensor code, as shown in the example Section.

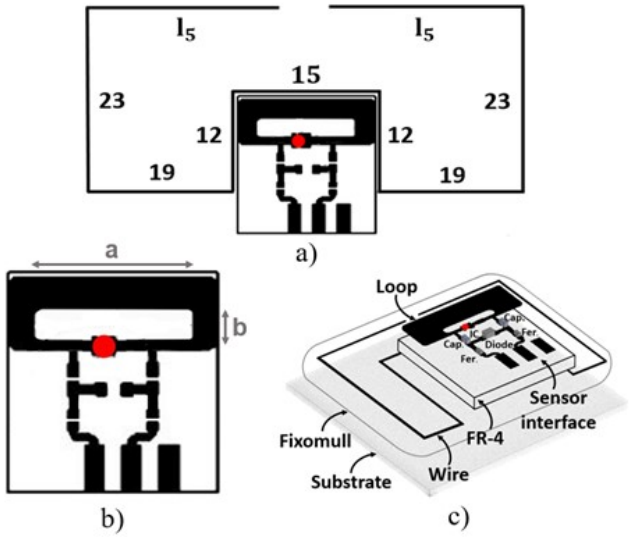

Fig. 4. a) Layout of the device (fixed sizes in [mm]); b) details of the loop-coupler with traces to host the electronic components and the pins for the sensor's connector; c) 3D view of the whole device including the wire meander-line dipole. Red circle indicates the RFID-IC.

IV. Application of the Method

The method is here demonstrated through the application to a typical pH sensor as in [9], namely a chemical multi-layering comprising three electrodes that are screen-printed on a polyethylene-terephthalate (PET) substrate (Fig.3).

The $pH - V_S$ curve can be approximated by the linear regression:

$$V_S = -0.0725pH + 0.7975. \tag{14}$$

By considering the pH range ($4 \leq pH \leq 8$), which includes typical human skin values, the corresponding output voltage range is ($0.2\,V \leq V_S \leq 0.5\,V$). The considered IC is the Axzon Magnus-S3 [19], with parameters $C_0 = 1pF/512$, $C_{min} = 1.9\,pF$, conductivity $G_{IC} = 0.482\,mS$, $S_{min} = 80$, $S_{max} = 400$, and nominal power sensitivity $p_{IC} = -16.6\,dBm$. The varactor diode is the SMV1405 by Skyworks Solution Inc., [18] with parameters $C_{j0} = 2.37\,pF$, $V_J = 0.77\,V$, and $M = 0.5$.

A. Antenna layout

The considered antenna layout and other interconnections are sketched in Fig.4. A meander-line copper dipole (wire diameter 0.08 mm) is deposited over a Fixomull (plaster-like adhesive substrate [20] (size 55 mm $\times$ 33.5 mm, thickness 0.22 mm) that is in turn placed over a forex (closed-cell PVC foamboard, $\epsilon_r = 1.55$, $\sigma = 0.0006\ S/m$) surface (size 100 mm $\times$ 100 mm, thickness 5 mm). The dipole is coupled to the IC through a loop transformer (over a 14.2 mm $\times$ 15.1 mm FR-4 ($\epsilon_r = 4.3$, $tan\delta = 0.025$) substrate, thickness 1.6 mm), in turn connected to the varactor. To prevent the diode from absorbing the RF signal coming from the reader, a proper RF decoupling is provided by two ferrite beads as in [17]. The free parameters for the design are $\underline{\alpha} = \{b, l_5, C_d\}$, the first one dominating the susceptance, the second one controlling the conductance and the latter adjusting the sensitivity of the whole system.

TABLE I
SENSOR CODE VALUES AND CONTRASTS FOR DIFFERENT DECOUPLING CAPACITANCES

c_d	s_{min}	s_{max}	Δ_s
12 pF	195	287	72
15 pF	172	258	86
18 pF	100	200	100

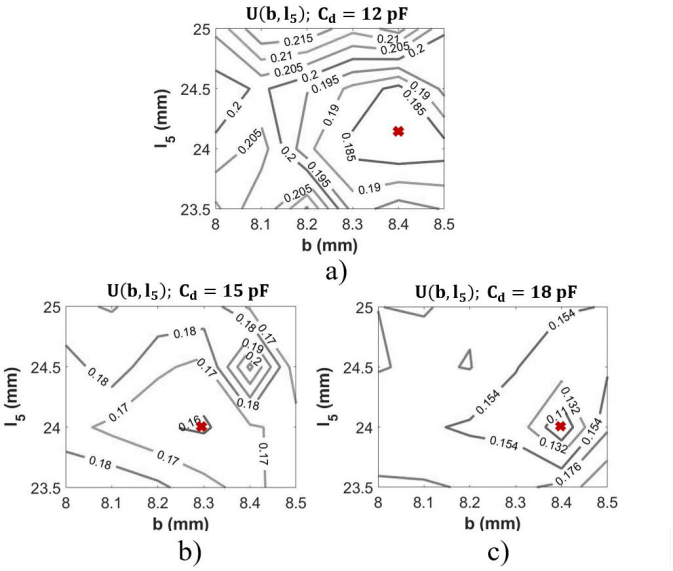

Fig. 5. Contour plots of the penalty function U(b,l_5) in (10-13) (lower is better) for a) C_d = 12 pF b) C_d = 15 pF and c) C_d = 18 pF. Red marker indicates the optimum configuration.

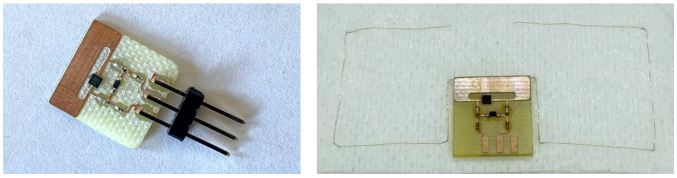

Fig. 6. Prototype of the device: a) PCB hosting the loop-coupler with the electronic components and the connector to plug the pH sensor in Fig.5; b) integration with the wire dipole antenna on an adhesive paper.

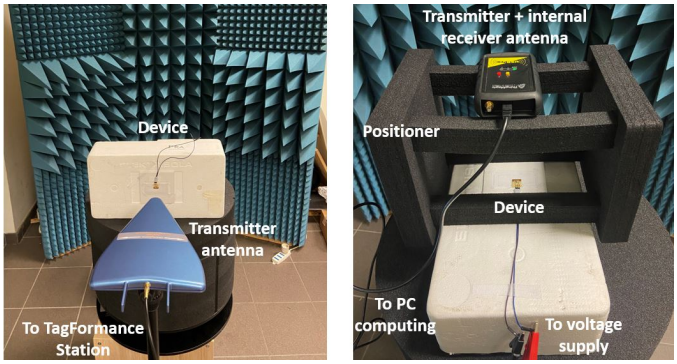

Fig. 7. Setup for electromagnetic characterization and sensor code measurements. The interrogation station was a) the Voyanting TagFormance connected to a linear polarized log-periodic antenna for the electromagnetic test, and b) the ThingMagic USB-Pro provided with an internal dipole-like antenna, for the sensing test.

B. Modeling

The radiation gain and impedance of the antenna that are required for the evaluation of the penalty function can be computed by following a hybrid numerical procedure, here exploiting the CST Microwave Studio simulator. In the first step, the whole device, including the radiating element and the copper traces, is modelled as an *N*-ports network, wherein the ports are associated with the terminals of the electronic elements (diode, IC, capacitors and ferrite beads), not included in the simulation. The impedance matrix and the radiation gain are computed by a full-wave solver (3D Finite Elements). In the second step, the interconnection with the electronic elements is evaluated offline by using a circuital tool (Schematic) that includes the accurate equivalent models of the electronic elements. The pH sensor is not considered in the simulations as it does not contribute to the RF behaviour of the device.

C. Simulation

As shown further on, the optimization is repeated for some values of the decoupling capacitance $C_d = \{12, 15, 18\}$ pF. The penalty functions U_i (pedix *i* referring to the above values of C_d) are shown in Fig.5 for $\{w_1, w_2, w_3, G_0\}$=$\{\frac{1}{4}, \frac{1}{4}, \frac{1}{2}, \frac{1}{10}\}$, wherein the antenna gain and admittance are evaluated at the European UHF frequency of 868 MHz. For each value of C_d, the optimal values of geometrical parameters are identified. The lowest penalty function is referred to the highest C_d value (Fig.5 c)). Table I shows the estimated values of sensor code $s_{min} = s(pH = 8)$ and $s_{max} = s(pH = 4)$ derived from (5) and the whole contrast $\triangle s$ for all three optimal geometries. The mapped window of sensor code is right inside the linear range. As expected, $\triangle s$ widens as the value of C_d increases, and in turn the device sensitivity as well.

Anyway, it is worth noticing that, even in the most favourable case, the achieved sensor code window (100-200) is narrower than the nominal range (80-400) of the IC due to the balance between sensing and communication performance in the optimization process. These results will be corroborated by the numerical experimentation in the next Section.

V. EXPERIMENTAL VALIDATION

The manufacturing of the prototype was carried out in three steps: *i)* the loop transformer was etched by a milling machine over a FR-4 PCB, *ii)* the electronic components (IC, diode, capacitances, and ferrite beads) were soldered with the help of a bench soldering iron and, *iii)* the wire antenna was laid down on an adhesive textile layer by the transfer technique introduced in [20]. The resulting device is shown in Fig.6.

A. Measurement setup and protocol

The experimental set-up comprised: *i)* a voltage generator to emulate the potentiometric sensor, then replaced by a real chemical sensor connected to the diode pads, *ii)* a circularly polarized antenna for interrogation, *iii)* the TagFormance UHF Pro station connected to the said antenna, and *iv)* some anechoic panels to reduce the enviromental reflections (Fig.7).

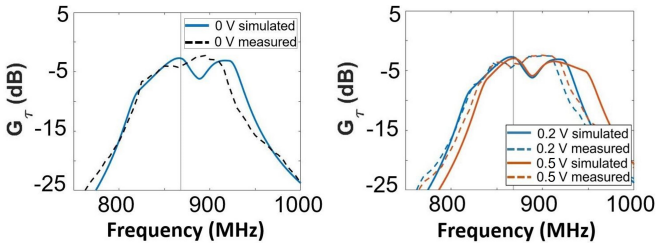

Fig. 8. Radiation performance of the device in free space: realized gain (broadside) in a) reference condition of $\boldsymbol{V_S = 0V}$ and b) for two applied voltages across the diode to emulate the potentiometric sensor.

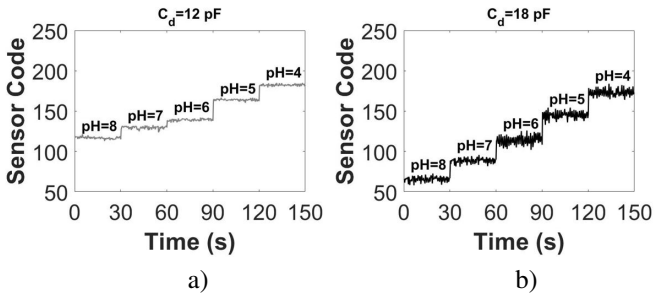

Fig. 9. Free space device: measured sensor code versus time for buffer solutions of different pH in case of a) $\boldsymbol{C_d = 12pF}$ and b) $\boldsymbol{C_d = 18pF}$.

From the measured turn-on power, the realized gain was preliminary derived, having emulated the sensor voltage, and then by connecting the pH sensor to the PCB.

Concerning the sensing characterization, the pH measurements were carried out by means of two identical devices having decoupling capacitances $C_d = \{12, 18\}$ pF respectively. The working electrode of the pH sensor was loaded by drops of an aqueous solution with a known pH. The devices were then interrogated for 30 seconds to collect several values of the sensor code and perform averaging. The experiments were repeated with liquid samples of different pH in the range $(4 \leq pH \leq 8)$. Between consecutive tests, the working electrode was cleaned to avoid artifacts.

From the obtained data, the regression curve and the relative sensitivity of the system were calculated.

B. Results

Fig.8 a) shows the realized gain when no voltage was applied (reference condition) whereas Fig.8 b) when voltages $[0.2\ V, 0.5\ V]$ were applied, to simulate respectively $pH = 8$ and $pH = 4$.
A good match with numerical simulations can be observed and above all, it is worth noticing that the communication performance is fully insensitive to the sensor voltage.

The step-wise response obtained by loading the sensor with different liquids, as above, is shown in Fig.9, wherein steps are related to liquids with different pH. There are some fluctuations of the sensor code around a stable baseline, that are smaller for the case of the smaller capacitor since they are naturally filtered out by the poorer resolution in the discretization process, as discussed in Section II.C. Fluctuations are a known effect [21] of the charge and discharge of the internal IC equivalent capacitor during the auto-tuning and can be removed by averaging. Overall, the change in the pH generates a distinguishable variation of the sensor code.

VI. Sensing Robustness vs. Placement Conditions: An Epidermal Application

The corresponding characteristic curves are reconstructed in Fig.10. The sensitivity can be hence computed as $S(C_d) = \frac{\triangle s}{\triangle pH}$ which rises as the decoupling capacitance C_d increases (Table II).

The method was finally applied to the design of an epidermal device that could be used for skin pH monitoring.

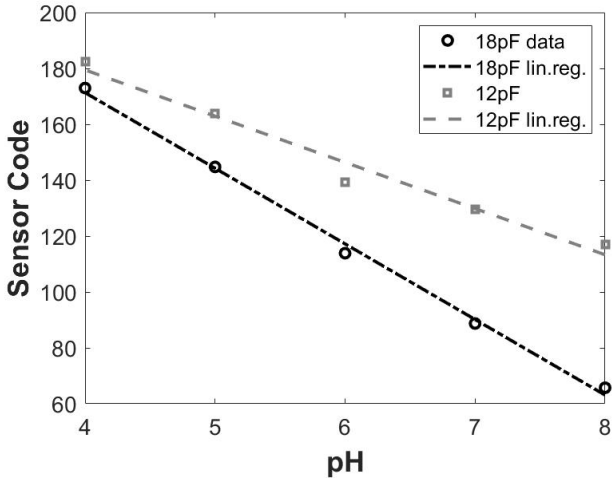

Fig. 10. Free space device: measured sensor code versus pH for $\boldsymbol{C_d = 12pF}$ and $\boldsymbol{C_d = 18pF}$. Linear regression superimposed.

TABLE II
MEASURED SENSOR CODE CONTRAST AND SENSITIVITY FOR TWO DECOUPLING CAPACITANCES

c_d	Δ_s	$S(C_d)$
12 pF	65	16.25
18 pF	117	29.25

This exercise will permit to evaluate the robustness of the sensing method when the device is used in not fully predictable conditions, namely the body region where it is attached and the inter-user variability.

A. Epidermal prototype

The layout of the antenna is similar to that in Fig.4 c) except for the placement on the skin instead of a forex substrate (Fig.11 a)). To increase biocompatibility, the copper traces were encapsulated within a medical-grade silicone layer (overall thickness of 2 mm). The decoupling capacitance was fixed at $C_d = 18pF$.

TABLE III
ELECTROMAGNETIC PROPERTIES OF HUMAN TISSUES AT 868 MHZ

Tissue	ε_r	$\sigma\,[Sm]$	t[mm]
Skin	41.57	0.86	1
Fat	5.47	0.05	10
Muscle	55.11	0.93	40

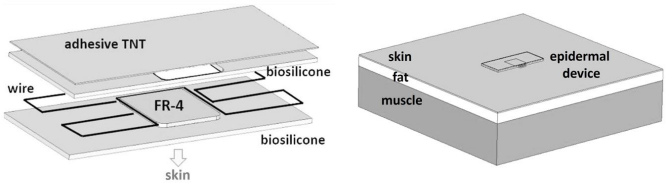

a) b)

Fig. 11. a) Exploded view of the simulated epidermal device placed onto a b) skin phantom.

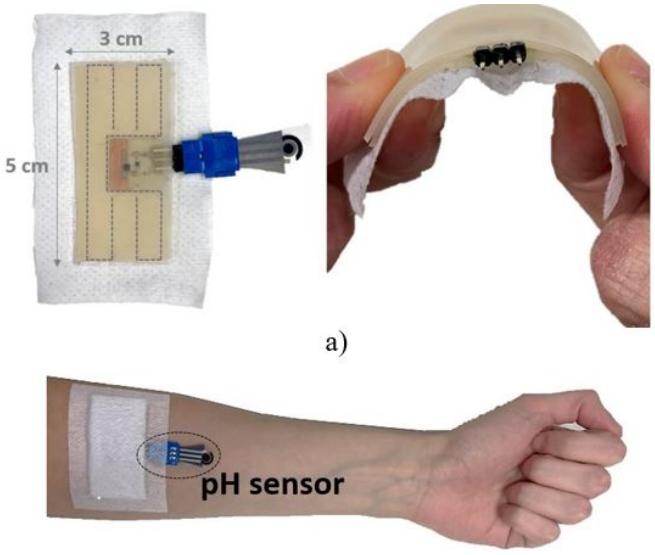

a)

b)

Fig. 12. a) The assembled epidermal prototype and b) its application over a forearm with the connection of the pH sensor.

Numerical simulations now include a layered human phantom (Fig.11 b)) with properties summarized in Table III [22]. The prototype is shown in Fig.12.

The resulting device is light, compact, flexible, and can therefore be conformally applied to body regions having different curvatures.

B. Measurement setup and protocol

The first experiments consisted of communication measurements by placing the device onto the human skin. The setup and data processing were the same as before. To quantify the robustness:

1) *with respect to the monitoring site*, the device was characterized on three different body areas with different curvatures of a same wearer (i.e. chest, arm, and just below the shoulder).
2) *with respect to the wearer*, the device was tested on the same body site for six people (details in Table IV);

Sensor code measurements were carried out by emulating the pH sensor with a voltage generator and the sensitivity of the device was evaluated. The characteristic curves were reconstructed from the measured data. To drop out the inter-user variability, the output sensor code s was normalized with respect to a reference value s_0, corresponding to the lowest voltage for each user, so that measurements on different wearers could be properly compared with each other.

TABLE IV
ELECTROMAGNETIC PROPERTIES OF HUMAN TISSUES AT 868 MHZ

wearer	sex	age	height [cm]	weight [kg]
f1	female	24	165	61
f2	female	25	167	63
f3	female	29	155	58
m1	male	25	167	64
m2	male	25	185	80
m6	male	25	172	74

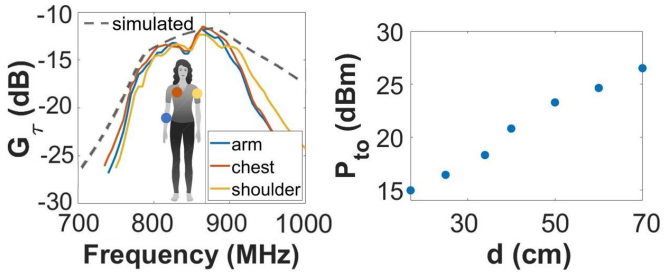

a) b)

Fig. 13. Epidermal device: a) measured realized gain in case of application on three body sites of a female volunteer, and comparison with the simulation in the reference condition. b) The average turn-on power versus the device-reader distance.

C. Results

The results for different body sites are shown in Fig.13 a) and prove a stable realized gain with respect to skin curvature. In particular, the average realized gain of -12 dB at the working frequency (868 MHz) is in good agreement with numerical simulations. Overall, in the UHF band, the realized gain is consistently greater than -15 dB, which represents a typical value for epidermal antennas [23], [24], [25], providing a read range of 70 cm by using a circular polarized reader antenna emitting 3.2 W EIRP (Fig.13 b)).

Concearning the inter-user variability, Fig.14 a) shows the realized gain measured over the six different wearers on the same site (the forearm) and only modest variations concearning each wearer are visible.

The $V - s$ curves are shown in Fig.14 b)) for a sub set of four volunteers. The increase in sensor code for a variation of 0.1 V is related to the slope $S(V)_0 = \frac{\triangle(s-s_0)}{\triangle V}$. Accordingly to the reference sensor calibration curve [6], by considering that a unitary change of pH corresponds to an increment of about 0.1 V, the sensitivity $S(pH)_0 = \frac{\triangle(s-s_0)}{\triangle pH}$ for each regression curve is estimated in Table V. The device is hence rather robust to the inter-user variability since the fluctuation of the sensitivity is of just one unit of sensor code for a unitary pH variation. Such oscillation is fully masked by the natural fluctuation of the sensor code.

VII. CONCLUSION

A constrained design method for RFID devices including auto-tuning ICs and potentiometric sensors has been introduced and validated. Its main advantage is the full control of the chemical to electromagnetic transduction, thus optimizing

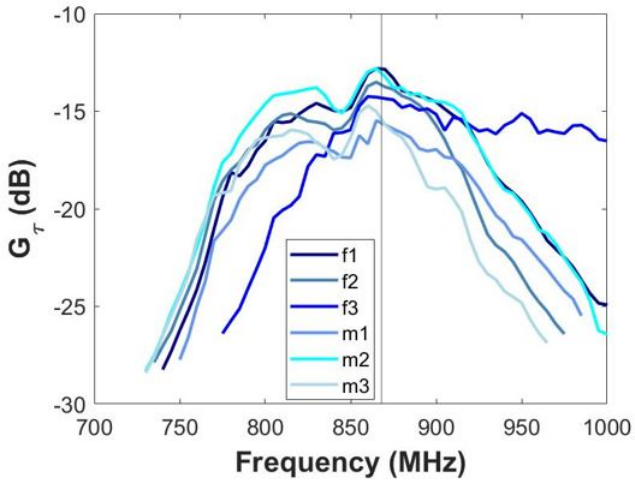

a)

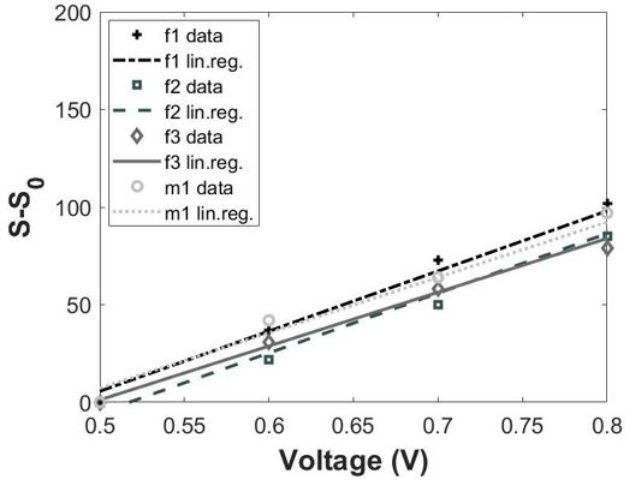

b)

Fig. 14. Epidermal device: a) measured realized gain for six wearers and b) normalized sensor code for three wearers versus the applied voltage.

TABLE V
ESTIMATED SENSITIVITY FOR ON-SKIN APPLICATION IN CASE OF FEMALE (f_1, f_2, f_3) AND MALE (m_1) USERS

	f1	f2	f3	m1	mean	std.
$S(V)_0$	308	292	278	288	291.8	10.8
$S(pH)_0$	30.8	29.2	27.8	28.8	29.2	1.1

the sensitivity of the device within the dynamic range of the physical phenomenon. As demonstrated in the application to on-skin antennas, the method permits to return a stable sensitivity even in case of not fully predictable boundary conditions. As the whole sensing chain has been parameterized, the design procedure can be applied to any potentiometric sensor thus likely boosting the application of auto-tuning RFID sensors to medical, food, pharma, and industrial domains.

Finally, by exploiting the paradigm of multi-chip RFIDs [26], the proposed architecture could be even simultaneously integrated with multiple chemical sensors to monitor more parameters at the same time, and hence provide a wider picture of the physical events.

VIII. Acknowledgment

The authors would like to thank PhD Student Luca Fiore and Professor Fabiana Arduini for collaborations, and RADIO6ENSE for technical support.

References

[1] Y. T. Konttinen, M. Takagi, J. Mandelin, J. Lassus, J. Salo, M. Ainola, T.-F. Li, I. Virtanen, M. Liljeström, H. Sakai *et al.*, "Acid attack and cathepsin k in bone resorption around total hip replacement prosthesis," *Journal of Bone and Mineral Research*, vol. 16, no. 10, pp. 1780–1786, 2001.

[2] M. Arifuzzaman, P. W. Millhouse, Y. Raval, T. B. Pace, C. J. Behrend, J. D. DesJardins, T.-R. J. Tzeng, and J. N. Anker, "Implanted chemical sensors for functional radiography," 2017.

[3] M.-H. Schmid-Wendtner and H. C. Korting, "The ph of the skin surface and its impact on the barrier function," *Skin pharmacology and physiology*, vol. 19, no. 6, pp. 296–302, 2006.

[4] G. Gethin *et al.*, "The significance of surface ph in chronic wounds," *Wounds uk*, vol. 3, no. 3, p. 52, 2007.

[5] L. A. Wallace, L. Gwynne, and T. Jenkins, "Challenges and opportunities of ph in chronic wounds," *Therapeutic delivery*, vol. 10, no. 11, pp. 719–735, 2019.

[6] V. Mazzaracchio, L. Fiore, S. Nappi, G. Marrocco, and F. Arduini, "Medium-distance affordable, flexible and wireless epidermal sensor for ph monitoring in sweat," *Talanta*, vol. 222, p. 121502, 2021.

[7] S. Mondal, S. Karuppuswami, and P. Chahal, "Id integrated batteryless wireless digital ph sensor," *IEEE Sensors Journal*, vol. 19, no. 24, pp. 12 079–12 086, 2019.

[8] W. Dang, L. Manjakkal, W. T. Navaraj, L. Lorenzelli, V. Vinciguerra, and R. Dahiya, "Stretchable wireless system for sweat ph monitoring," *Biosensors and Bioelectronics*, vol. 107, pp. 192–202, 2018. [Online]. Available: https://www.sciencedirect.com/science/article/pii/S0956566318301131

[9] S. Nappi, V. Mazzaracchio, L. Fiore, F. Arduini, and G. Marrocco, "Flexible ph sensor for wireless monitoring of the human skin from the medimun distances," in *2019 IEEE International Conference on Flexible and Printable Sensors and Systems (FLEPS)*. IEEE, 2019, pp. 1–3.

[10] M. C. Caccami and G. Marrocco, "Electromagnetic modeling of self-tuning rfid sensor antennas in linear and nonlinear regimes," *IEEE Transactions on Antennas and Propagation*, vol. 66, no. 6, pp. 2779–2787, 2018.

[11] K. Zannas, H. El Matbouly, Y. Duroc, and S. Tedjini, "Self-tuning rfid tag: A new approach for temperature sensing," *IEEE Transactions on Microwave Theory and Techniques*, vol. 66, no. 12, pp. 5885–5893, 2018.

[12] G. M. Bianco, S. Amendola, and G. Marrocco, "Near-field constrained design for self-tuning uhf-rfid antennas," *IEEE Transactions on Antennas and Propagation*, vol. 68, no. 10, pp. 6906–6911, 2020.

[13] G. M. Bianco, N. Panunzio, and G. Marrocco, "Rfid research against covid-19 – sensorized face masks," in *2021 IEEE International Conference on RFID Technology and Applications (RFID-TA)*, 2021, pp. 241–243.

[14] I. Ullah, R. Horne, B. Sanz-Izquierdo, and J. C. Batchelor, "Rfid ac current sensing technique," *IEEE Sensors Journal*, vol. 20, no. 4, pp. 2197–2204, 2020.

[15] A. Hillier, V. Makarovaite, S. J. Holder, C. W. Gourlay, and J. C. Batchelor, "A passive uhf rfid ph sensor (smart polymers for wireless medical sensing devices)," in *Loughborough Antennas Propagation Conference (LAPC 2017)*, 2017, pp. 1–2.

[16] A. J. Hillier, V. Makarovaite, C. W. Gourlay, S. J. Holder, and J. C. Batchelor, "A passive uhf rfid dielectric sensor for aqueous electrolytes," *IEEE Sensors Journal*, vol. 19, no. 14, pp. 5389–5395, 2019.

[17] F. Nanni, S. Nappi, and G. Marrocco, "Potentiometric sensing by means of self-tuning rfid ics," in *2022 IEEE International Conference on RFID (RFID)*, 2022, pp. 17–22.

[18] S. to SMV1430 Series, "Plastic Packaged Abrupt Junction Tuning Varactors Datasheet," www.skyworksinc.com.

[19] Axzon, "RRFM3300-E Magnus-S3 M3E passive sensor IC," https://axzon.com/rfm3300-e-magnus-s3-m3e-passive-sensor-ic/, September 2021.

[20] C. Miozzi, F. Amato, and G. Marrocco, "Performance and durability of thread antennas as stretchable epidermal uhf rfid tags," *IEEE Journal of Radio Frequency Identification*, vol. 4, no. 4, pp. 398–405, 2020.

[21] F. Camera and G. Marrocco, "Electromagnetic-based correction of bio-integrated rfid sensors for reliable skin temperature monitoring," *IEEE Sensors Journal*, vol. 21, no. 1, pp. 421–429, 2021.
[22] I. I. N. R. Council, "Dielectric properties of body tissues in the frequency range 10 hz - 100 ghz," April 2022, available on line.
[23] S. Manzari, S. Pettinari, and G. Marrocco, "Miniaturised wearable uhf-rfid tag with tuning capability," *Electronics letters*, vol. 48, no. 21, pp. 1325–1326, 2012.
[24] S. Amendola and G. Marrocco, "Optimal performance of epidermal antennas for uhf radio frequency identification and sensing," *IEEE Transactions on Antennas and Propagation*, vol. 65, no. 2, pp. 473–481, 2017.
[25] M. C. Caccami, M. Y. S. Mulla, C. Occhiuzzi, C. Di Natale, and G. Marrocco, "Design and experimentation of a batteryless on-skin rfid graphene-oxide sensor for the monitoring and discrimination of breath anomalies," *IEEE Sensors Journal*, vol. 18, no. 21, pp. 8893–8901, 2018.
[26] C. Occhiuzzi, S. Parrella, F. Camera, S. Nappi, and G. Marrocco, "Rfid-based dual-chip epidermal sensing platform for human skin monitoring," *IEEE Sensors Journal*, vol. 21, no. 4, pp. 5359–5367, 2021.

Francesca Nanni received the B.S. and M.S. degree in Medical Engineering (Hons.) from the University of Rome Tor Vergata, Rome, Italy in 2019 and 2022, respectively. She is starting to pursue the Ph.D. degree in Computer Science, Control and Geoinformation within the Pervasive Electromagnetics Lab at the University of Rome Tor Vergata, Rome, Italy.

Ms. Nanni's research focuses on radio-mechanical digital twins and how to apply machine learning and artificial intelligence algorithms to design robust and versatile body antennas.

She is also part of the Cyber4Health project, which raises international awareness about the need to apply Cyber and Physical security by design in medical devices.

She has been a coauthor of the paper "Cyber-tooth: Antennified dental Implant for RFID Wireless temperature Monitoring" winner of the Best Student Paper Award at the 2021 IEEE International Conference on RFID Technology and Applications (RFID-TA 2021). She also won the Best Student Paper Award at the 2022 IEEE International Conference on RFID Technology and Applications (RFID-TA 2022).

Gaetano Marrocco received the M.S. degree in Electronic Engineering and Ph.D. degree in Applied Electromagnetics from the University of L'Aquila, L'Aquila, Italy in 1994 and 1998, respectively. He was a Researcher at the University of Rome Tor Vergata, Rome, Italy from 1994 to 2014. He was an Associate Professor of Electromagnetics from 2013 to 2017, and a Full Professor at the University of Rome Tor Vergata since 2018. He currently serves as Director of the Medical Engineering School.

The first phase of his career was devoted to the research on Time-Domain Electromagnetics with application to structural, broadband, and ultra-wideband antennas for Satellite (ESA, ASI), Avionic, and Naval (Leonardo) communications. Then, since 2002, he is investigating sensor-oriented miniaturized antennas for Biomedical Engineering and Radiofrequency Identification (RFID), contributing to the move from the RF labeling of objects to the passive sensor networks in the Internet of Things era. He carried out pioneering research on body-centric battery-less wireless sensors concerning textile RFID antennas, tattoo-like sensors (flexible and stretchable epidermal electronics), and radio-sensors embedded inside implanted prostheses.

He serves as Associate Editor for the IEEE Journal of Radiofrequency Identification and for the IEEE Journal of Flexible Electronics and was a member of the IEEE Antennas and Propagation Society Awards committee. Moreover, he is the chair of the Italian delegation URSI Commission D Electronics and Photonics. He was the chair of the Local Committee of the V European Conference on Antennas and Propagation (EUCAP-2011), TPC chair of the 2012 IEEE-RFID TA in Nice, France, TPC track-chair of the 2016 IEEE Antennas and Propagation Int. Symposium, TPC track-chair of IEEE-RFID 2018-22, USA.

Prof. Marrocco is the director of the Pervasive Electromagnetics Lab (www.pervasive.ing.uniroma2.it) and the co-founder and president of the University spin-off RADIO6ENSE (www.radio6ense.com), which is active in the short-range electromagnetic sensing for the Industrial Internet of Things, Smart Manufacturing, Automotive and Medical Device.

He is listed in the PLOS ranking of Top 2% Scientists Worldwide (source Univ. Stanford, 2022).